Chapter 2
Multidimensional Spectroscopy: Concepts

Richard R. Ernst

Laboratorium für Physikalische Chemie, Eidgenössische Technische Hochschule, 8093 Zürich, Switzerland

2.1 INTRODUCTION

Two-dimensional and multidimensional spectroscopy are more than just another minor variant of the well-known, and old-fashioned, one-dimensional spectroscopy. Two-dimensional spectroscopy reveals a new general concept of experimental design which has opened up access to an astoundingly rich world of novel pulse experiments.[1–4] The principles of two-dimensional spectroscopy are in no way limited to NMR, and apply to all combinations of spectroscopic domains. However, they are most easily exemplified in NMR and have there found their most fruitful playground.

A large number of inventive and ingenious physicists and chemists have paved the way towards two-dimensional spectroscopy. Already the basic Hahn spin echo experiment bears the germ for 2D spectroscopy.[5] But, unquestionably, the most significant contribution has been made by Jean Jeener who is the actual creator of 2D spectroscopy.[6]

This brief chapter cannot be exhaustive and cannot do justice to all meritorious contributors who are responsible for the discovery and development of this new world of spectroscopy. Rather, the aim is to illuminate some general concepts underlying multidimensional spectroscopy which have revolutionized NMR, as an introduction to further, more specialized chapters in this book.

2.2 SPECTROSCOPY

The ultimate goal of spectroscopy is the exploration of (black box) systems by means of input/output relationships, as shown in Figure 2.1.[1] In its most elementary form, it provides the frequency response or transfer function $H(\omega)$ that measures the (complex) transfer characteristics of a linear time-invariant system Φ when perturbed by the variable frequency ω or, more exactly, by its exponential function $\exp(i\omega t)$:

$$\hat{\Phi} \exp(i\omega t) = H(\omega) \exp(i\omega t) \qquad (2.1)$$

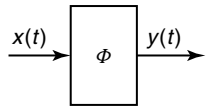

Figure 2.1. Input/output relationship for a system Φ with the input function $x(t)$ and the output function $y(t)$.

This equation implies that the exponential functions $\exp(i\omega t)$ are eigenfunctions of all linear and time-invariant systems or system operators $\hat{\Phi}$. The continuous sequence of 'eigenvalues' represents the transfer function or the complex spectrum $H(\omega)$.

This immediately leads to the general spectroscopic recipe: apply a sinusoidal perturbation of frequency ω to the linear time-invariant system, measure the amplitude $H(\omega)$ of the sinusoidal response, vary the frequency, and plot $H(\omega)$ (or its real and imaginary parts) as a function of the frequency ω to obtain a spectrum.

In some cases, spectroscopy is used for the measurement of the emission characteristics of a source of spontaneous radiation, in the absence of an external perturbation. Then a frequency-selective (dispersive) element is required in the detector, and the frequency dependence is introduced by varying this dispersive element. This type of emission spectroscopy is common in astronomy, in optical flame spectroscopy, and in NMR spin-noise measurements.[7,8] It is not considered further in this chapter, which is restricted to measurements of input/output relationships.

In a generalized version of spectroscopy, several simultaneous sinusoidal perturbations of different frequencies and several simultaneous detectors tuned to these frequencies are conceivable. This leads either to the multiple channel spectroscopy experiment (Figure 2.2), in which the linear response character of the system is maintained,

$$\hat{\Phi}\left[\sum_k \exp(i\omega_k t)\right] = \sum_k H(\omega_k)\exp(i\omega_k t) \quad (2.2)$$

or to double or multiple resonance (Figure 2.3) when interference between the different frequencies becomes essential in a nonlinear response system, as is typical for magnetic resonance of coupled spins.[9–11]

Another form of generalized spectroscopy is the measurement of the impulse response $h(t)$, which is the response to a delta-function perturbation:

$$\hat{\Phi}[\delta(t)] = h(t) \quad (2.3)$$

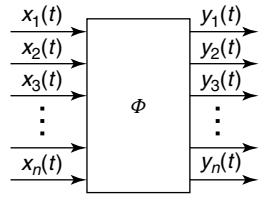

Figure 2.2. Multiple channel spectroscopy. For a linear system Φ, several simultaneous perturbations may be applied, and their response detected without mutual interference.

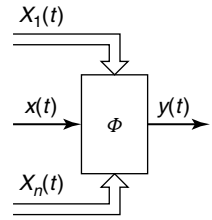

Figure 2.3. Multiple resonance experiment. The nonlinear system Φ is perturbed by several strong perturbations $X_1(t)$ ... $X_n(t)$ while the response of a weak perturbation $x(t)$ is observed.

The delta function $\delta(t)$ represents an equally weighted superposition of all frequencies:

$$\delta(t) = \frac{1}{2\pi}\lim_{\Omega\to\infty}\int_{-\Omega}^{\Omega}\exp(i\omega t)\,d\omega \quad (2.4)$$

and the impulse-response measurement is the ultimate form of multiple channel spectroscopy. For a linear time-invariant system, the important FT relationships

$$H(\omega) = \int_{-\infty}^{\infty} h(t)\exp(-i\omega t)\,dt \quad (2.5)$$

and

$$h(t) = \frac{1}{2\pi}\int_{-\Omega}^{\Omega} H(\omega)\exp(i\omega t)\,d\omega \quad (2.6)$$

hold, and it is possible to compute from the measured impulse response or FID, $h(t)$, the frequency response function or the complex spectrum, $H(\omega)$. This leads to pulse FT spectroscopy.[12–15] The inherent sensitivity advantage of this most important multiple channel experiment is obvious and has been well documented.

In frequency domain spectroscopy, the excitation, the evolution of the system to be investigated, and

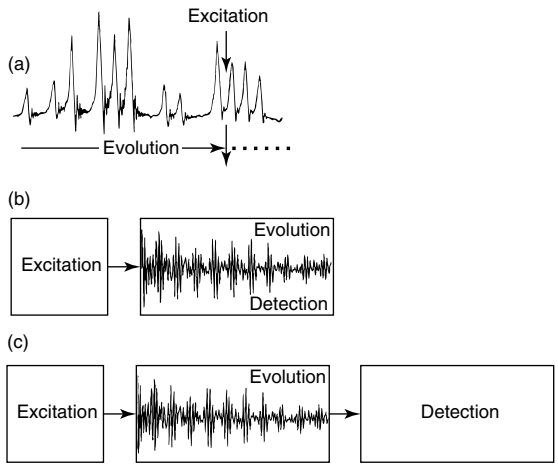

Figure 2.4. Three stages of sequential experimental design. (a) Simultaneous excitation, evolution, and detection in CW spectroscopy. (b) Simultaneous evolution and detection after an initial excitation in pulse FT spectroscopy. (c) Sequentially separated excitation, evolution, and detection provide the germ for multidimensional experiments.

the detection, occur simultaneously [Figure 2.4(a)]. This limits the degrees of freedom of experimental design and the number of possible spectroscopic experiments. In pulse FT spectroscopy, the excitation process has been detached and the evolution occurs in the absence of any perturbation [Figure 2.4(b)]. This has great inherent advantages. First, the excitation can take arbitrary forms such as variable flip angle pulses, $(\pi-\tau-\pi/2)$ inversion–recovery excitation, $(\pi/2-\tau/2-\pi-\tau/2)$ spin echo excitation, excitation by heteronuclear polarization transfer, and many more. Second, the free evolution in the absence of a rf field leads to the most faithful representation of the spectral properties of the system investigated.

2.3 TWO-DIMENSIONAL AND MULTIDIMENSIONAL SPECTROSCOPY

Multidimensional spectroscopy carries to the extreme the separation of the independent units of a spectroscopic experiment as shown in Figure 2.4(c). The three parts–excitation, evolution, and detection–are the basic building blocks of any multidimensional spectroscopy experiment.[1,16] All three parts are

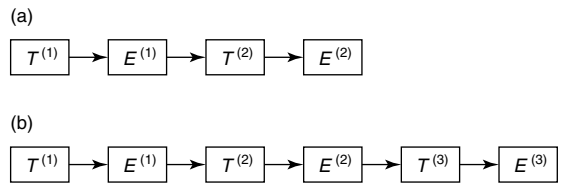

Figure 2.5. Prototype two- (a) and three-dimensional (b) experiments consisting of an alternating sequence of transfer and evolution blocks. Each evolution block provides a time variable that leads, after FT, to a frequency dimension in the multidimensional spectrum.

indispensable. The excitation process is required for the creation of a nonequilibrium state with a density operator that does not commute with the Hamiltonian and, consequently, evolves over time. The evolution period is necessary for putting into evidence the spectral features of the investigated system. Without the detection process, the experiment would remain unnoticed. The separation of evolution and detection also allows the observation of features which are not detectable directly, such as the evolution of multiple quantum coherences.

Having separated the basic building blocks, they can be tailored individually and then combined to give arbitrarily complex experiment sequences. In the following we distinguish between just two general types of building blocks: evolution blocks E, and transfer blocks T (Figure 2.5).

2.3.1 The Evolution Blocks *E*

During an evolution period $E^{(r)}$, the density operator evolves under the guidance of a system Hamiltonian $\hat{\mathcal{H}}$, which may represent the unperturbed Hamiltonian $\hat{\mathcal{H}}_0$ of the system, $\hat{\mathcal{H}}_0 = \hat{\mathcal{H}}_{\mathrm{I}} + \hat{\mathcal{H}}_{\mathrm{II}} = \Sigma_k\, \Omega_k \hat{I}_{kz} + \Sigma_{k<l}\, \Sigma\, 2\pi J_{kl} \hat{I}_k \hat{I}_l$ (we address, for simplicity, only isotropic liquids). This can also be a Hamiltonian modified by a static perturbation, such as by an additional static or rf magnetic or electric field, or by a periodic or aperiodic perturbation, leading to an average Hamiltonian $\hat{\bar{\mathcal{H}}}_r$ that governs the overall time evolution of the density operator during the interval t_r:

$$\hat{\sigma}(t_r) = \exp(-\mathrm{i}\hat{\bar{\mathcal{H}}}_r t_r)\, \hat{\sigma}(t_r = 0) \exp(\mathrm{i}\hat{\bar{\mathcal{H}}}_r t_r) \quad (2.7)$$

Each evolution period introduces an additional time parameter t_r which can be varied systematically for

putting into evidence the spectral features of the Hamiltonian $\hat{\tilde{\mathcal{H}}}_r$. For simplicity, relaxation is disregarded in equation (2.7).

The evolution blocks provide, in general, spectral information, either in the sense of standard spectroscopy, to characterize the spectral response properties of the investigated system, or for the state identification before and after a coherence transfer step by 'frequency labeling'. The visualization of the spectral features during the period $E^{(r)}$ requires a FT of the detected response $h(\ldots, t_r, \ldots)$ as a function of t_r, thereby introducing an additional frequency variable ω_r in the spectrum $H(\ldots, \omega_r, \ldots)$. Obviously, the number of evolution periods with adjoint FT determines the dimension of the resulting multidimensional spectrum.

The last evolution period serves for detection. Usually, but not necessarily, it also provides additional spectral information in the sense of conventional FT spectroscopy. Sometimes, only a single sample value is taken during the last 'evolution' period as a measure of the preceding evolutions and transformations.

2.3.2 The Transfer Blocks *T*

A transfer block $T^{(r)}$ serves for the (virtually instantaneous or extended-time) transformation of the density operator, either by a unitary process

$$\hat{\sigma}'' = \hat{T}_r \hat{\sigma}' \hat{T}_r^{-1} \tag{2.8}$$

with the unitary transformation operator or propagator $\hat{T}_r$, or by a dissipative relaxation or chemical exchange process

$$\hat{\sigma}(\tau_r) = \hat{\sigma}(0) - \exp(-\hat{\tilde{\Gamma}}_r \tau_r)\,[\hat{\sigma}(0) - \hat{\sigma}_0] \tag{2.9}$$

with the relaxation or chemical exchange superoperator $\hat{\tilde{\Gamma}}_r$. Often, both unitary and dissipative processes occur at the same time during a transfer period $T^{(r)}$.

The transfer time τ_r of a mixing period r is usually kept constant in order to obtain a determined transfer behavior. In special situations, τ_r may be incremented in accordance with an evolution time t_s, such as in the accordion experiment.[17] In other cases, τ_r may be varied within a set of experiments, for example to visualize the build-up of transferred spin order in a cross relaxation or chemical exchange study.

A general multidimensional experiment can be conceived of as a sequence of specific T and E building blocks. Prototype two- and three-dimensional experiments are shown in Figure 2.5. Each multidimensional experiment starts with a T block that creates the required initial nonequilibrium state and ends with an E block for detection of the response signal. In between, an arbitrary sequence of E and T blocks can be arranged. The immediate succession of two E blocks, E_k and E_l, makes sense only when the two (average) Hamiltonians $\hat{\tilde{\mathcal{H}}}_k$ and $\hat{\tilde{\mathcal{H}}}_l$ are unequal. Immediately adjacent T blocks make sense only when they are distinct, effecting two different kinds of transfer or transformation or when they are subjected to unequal phase cycling procedures. Otherwise, no restrictions are imposed upon the sequence of building blocks. Two fairly complex examples, shown in Figure 2.10, are discussed later in this chapter.

2.4 COHERENCE TRANSFER PATHWAY SELECTION

The proper selection of coherence transfer pathways in multidimensional spectroscopy is at least as important as the proper sequence of building blocks.[1,18,19] Coherence is defined in the present context as a linear superposition of two eigenfunctions $|\phi_k\rangle$ and $|\phi_l\rangle$ of the system Hamiltonian $\hat{H}$ with the corresponding eigenvalues E_k and E_l:

$$\begin{aligned}\Psi_{kl}(t) = {} & c_k|\phi_k\rangle \exp(\mathrm{i}E_k t/\hbar) \\ & + c_l|\phi_l\rangle \exp(\mathrm{i}E_l t/\hbar)\end{aligned} \tag{2.10}$$

Coherence is reflected in the density matrix, written in the eigenbasis of the Hamiltonian, by the presence of the off-diagonal elements σ_{kl} and σ_{lk}. The contribution of coherence between states $|\phi_k\rangle$ and $|\phi_l\rangle$ to the density operator $\hat{\sigma}$ can also be written in the form

$$|k\rangle\langle l|(t) = |\phi_k\rangle\langle\phi_l| \exp[-\mathrm{i}(E_k - E_l)t/\hbar] \tag{2.11}$$

Coherence signifies a 'transition in progress' or the 'precession of transverse spin order' which possibly leads to transverse magnetization precessing, with the difference frequency $\omega_{kl} = (E_k - E_l)/\hbar$.

During the course of an E block, a coherence component (in the basis of the momentary Hamiltonian) retains its identity. However, the transfer blocks T transfer coherence between different components. They are therefore responsible for the coherence transfer and for the coherence-transfer pathways.

Based on equation (2.8), for example, one can express the coherence component σ_{pq}'' after transfer in terms of the coherence components σ_{kl}' before transfer:

$$\sigma_{pq}'' = \sum_{kl} (T_{pk} T_{lq}^{-1}) \sigma_{kl}' \tag{2.12}$$

assuming equal Hamiltonians before and after the transfer.

Most magnetic resonance experiments are performed under high magnetic field conditions where the magnetic quantum number M_k, defined as an eigenvalue of $\hat{F}_z$, is a good quantum number:

$$[\hat{\mathcal{H}}_0, \hat{F}_z] = 0 \tag{2.13}$$

and

$$\hat{F}_z |k\rangle = M_k |k\rangle \tag{2.14}$$

with $\hat{F}_z = \Sigma_p \hat{I}_{pz}$ where the summation p extends over all spins I_p of the system. Often, the average Hamiltonians $\hat{\bar{\mathcal{H}}}_k$ of the various evolution periods E_k also commute with $\hat{F}_z$,

$$[\hat{\bar{\mathcal{H}}}_k, \hat{F}_z] = 0 \tag{2.15}$$

and the corresponding coherences $|k\rangle\langle l|$ can be characterized by 'good' magnetic quantum numbers p_{kl}:

$$[|k\rangle\langle l|, \hat{F}_z] = p_{kl} |k\rangle\langle l| \tag{2.16}$$

with

$$p_{kl} = M_k - M_l \tag{2.17}$$

Based on the quantum number p_{kl}, coherences are classified in coherence orders with zero quantum coherences ($p_{kl} = 0$), ± 1 quantum coherences ($p_{kl} = \pm 1$), ± 2 quantum coherences ($p_{kl} = \pm 2$), etc.

The sequence of coherence orders that appears over the course of time is characteristic of the behavior of a multidimensional spectroscopy experiment. Several experiments involve the same pulse sequence and differ only in the sequence of appearance of the coherence orders. For example, relayed COSY, multiple quantum filtered COSY, and NOESY all use a sequence of three $\pi/2$ pulses, but select different coherence transfer pathways. It is thus necessary to provide a means for selecting coherence transfer pathways during the course of a pulse experiment.

Two general procedures are known for the selection of coherence orders. The first one is based on the transformation properties of coherences under z rotations.[20] With equation (2.16), one finds that a z rotation by the angle ϕ multiplies a coherence $|k\rangle\langle l|$ by a phase factor:

$$\begin{aligned} &\exp(-\mathrm{i}\phi \hat{F}_z)\, |k\rangle\langle l| \exp(\mathrm{i}\phi \hat{F}_z) \\ &\quad = \exp(-\mathrm{i} p_{kl} \phi)\, |k\rangle\langle l| \end{aligned} \tag{2.18}$$

Let us assume that a transfer block T in an experiment is phase shifted by incrementing the phase of the involved rf pulses by ϕ. The new propagator $\hat{T}_\phi$ can then be expressed as

$$\hat{T}_\phi = \exp(-\mathrm{i}\phi \hat{F}_z)\, \hat{T} \exp(\mathrm{i}\phi \hat{F}_z) \tag{2.19}$$

i.e. by two phase-shifting operations bracketing the original propagator.

We assume a general coherence transfer

$$\hat{T} |k\rangle\langle l| \hat{T}^{-1} = \sum_{m,n} a_{mn} |m\rangle\langle n| \tag{2.20}$$

and apply the phase shift ϕ:

$$\begin{aligned} &\hat{T}_\phi |k\rangle\langle l| \hat{T}_\phi^{-1} \\ &\quad = \sum_{m,n} a_{mn} |m\rangle\langle n| \exp[-\mathrm{i}(p_{mn} - p_{kl})\phi] \end{aligned} \tag{2.21}$$

In order to select the transfers with a specific change Δp in coherence order, it is possible to take advantage of the orthogonality of the Fourier series and to perform a series of N experiments with the phases

$$\phi_j = j 2\pi / N \tag{2.22}$$

and to form a weighted linear combination of the results:

$$\begin{aligned} \sum_{j=0}^{N-1} &\exp(\mathrm{i}\Delta p \phi_j)\, \hat{T}_{\phi_j} |k\rangle\langle l| \hat{T}_{\phi_j}^{-1} = \sum_{m,n} a_{mn} |m\rangle \\ &\times \langle n| \sum_{j=0}^{N-1} \exp[-\mathrm{i}(p_{mn} - p_{kl} - \Delta p)\phi_j] \\ = &\sum_{m,n} a_{mn} |m\rangle\langle n| N \\ &\times \sum_{q=-\infty}^{\infty} \delta_{p_{mn} - p_{kl}, \Delta p + qN} \end{aligned} \tag{2.23}$$

The sum over q represents the usual aliasing problem of Fourier series which renders indistinguishable coherences that differ in their order by qN. If N is selected to be sufficiently large, the aliased higher coherence orders can be disregarded, and equation (2.23) then expresses a unique selection of coherence transfer with $p_{mn} - p_{kl} = \Delta p$, as desired.

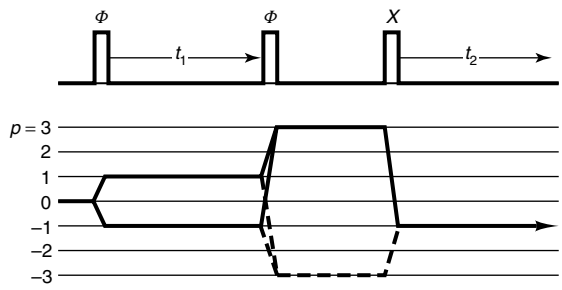

Figure 2.6. Coherence transfer pathways in three quantum filtered COSY. A six-step phase cycle ($\phi = k\pi/3$, $k = 0, \ldots, 5$) of the first two pulses selects a triple quantum coherence which is converted by the third pulse to a $p = -1$ coherence that is selected and measured by quadrature phase detection. To obtain pure phase peak shapes, it is necessary to retain the $p = \pm 1$ coherence during the evolution period t_1. To distinguish between positive and negative ω_1 frequencies, four-step time proportional phase incrementation (TPPI)[21] is applied to all three pulses.

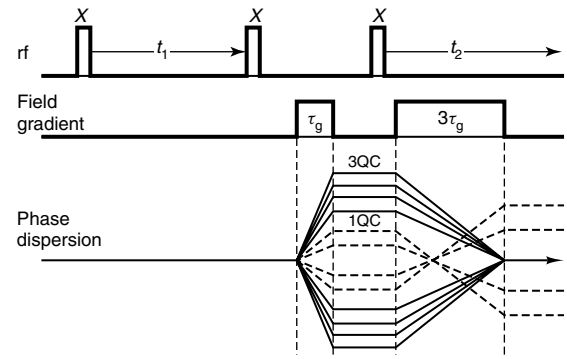

Figure 2.7. Coherence transfer pathway selection in three quantum filtered COSY by magnetic field gradient pulses (gradient-enhanced spectroscopy). The phase dispersion initiated by the first gradient pulse of duration τ_g is shown for $p = +1$ (----) and $p = +3$ quantum coherence (—). The refocusing time for the observed $p = -1$ quantum coherence depends on the amount of phase dispersion acquired. The former three quantum coherence components fully refocus at the end of the second gradient pulse of duration $3\tau_g$. Only the pathway $p = +3 \rightarrow p = -1$ is selected (solid lines in Figure 2.6), while the pathway $p = -3 \rightarrow p = -1$ (broken lines in Figure 2.6) is suppressed. A TPPI phase cycle on all pulses is required for the distinction of positive and negative ω_1 frequencies.

Equation (2.23) is the foundation of phase cycling procedures where the linear combination of N experiments selects a predetermined value Δp. Provided that the initial coherence order p_{kl} is known, it is also possible in this manner to select a definite final value p_{mn}. The most convenient procedure for selecting the coherence order at a particular instant in a pulse experiment is to apply a phase cycle to all preceding pulses, knowing that the initial state of the spin system had coherence order $p_{kl} = 0$. Often, several independent phase cycles applied to different pulses or pulse sequences are required to select the desired coherence transfer pathway in a particular experimental situation.[1,19] The pathways for a triple quantum filtered COSY experiment, shown in Figure 2.6, serve as an example.

A second procedure for coherence transfer pathway selection (often called 'gradient-enhanced spectroscopy') exploits the different sensitivity of coherence orders to magnetic field inhomogeneity pulses.[22–24] A spatially inhomogeneous magnetic field with the gradient $\boldsymbol{g}_r$ and the local Zeeman frequency deviation at coordinate $\boldsymbol{x}$,

$$\Delta\omega_r(\boldsymbol{x}) = \boldsymbol{g}_r \cdot \boldsymbol{x} \tag{2.24}$$

applied for a time τ_j to a coherence $|k\rangle\langle l|$, leads to a phase distribution according to

$$\begin{aligned} &\exp(-\mathrm{i}\boldsymbol{g}_r \cdot \boldsymbol{x}\hat{F}_z\tau_r)\,|k\rangle\langle l|\exp(\mathrm{i}\boldsymbol{g}_r \cdot \boldsymbol{x}\hat{F}_z\tau_r) \\ &\quad = |k\rangle\langle l|\exp(-\mathrm{i}p_{kl}\boldsymbol{g}_r \cdot \boldsymbol{x}\tau_r) \end{aligned} \tag{2.25}$$

Obviously the phase dispersion is weighted by the coherence order p_{kl}. The higher the order of the coherence, the larger is the resulting spread in the phase distribution (Figure 2.7).

A cumulative dephasing $\phi(\boldsymbol{x})$ occurs during the course of a sequence of coherence transfers with the coherence orders $\{p_r\}$ (p_r standing for p_{kl}) when a sequence of field gradient pulses with the gradients $\boldsymbol{g}_r$ is applied for the time periods τ_r:

$$\phi(\boldsymbol{x}) = \sum_r p_r \boldsymbol{g}_r \cdot \boldsymbol{x}\tau_r \tag{2.26}$$

Whenever $\phi(\boldsymbol{x}) \equiv 0$, the dephasing will be fully refocused and a coherence transfer echo occurs.

In gradient-enhanced spectroscopy, a sequence of gradient pulses is selected such that only for the chosen coherence transfer pathway $\{p_1, p_2, \ldots, p_n\}$ does an echo occur at the instant of measurement. This requires that

$$\sum_{r=1}^{n} p_r \boldsymbol{g}_r \tau_r = 0 \tag{2.27}$$

while for all other sequences of coherence orders this expression should remain different from zero. If such a sequence of values $\{\boldsymbol{g}_r\tau_r\}$ is found, the goal has been reached and the coherence transfer pathway $\{p_1, p_2, \ldots, p_n\}$ has been uniquely selected.

Three quantum filtered COSY can serve again as an example (Figure 2.7). The selection of coherence order is made before and after the third pulse. The $p = 3$ quantum defocusing during the first gradient pulse of duration τ_g occurs three times as fast as for the $p = 1$ quantum coherence. The refocusing time of a coherence $p = -1$ is proportional to the degree of previous dephasing. Only the initial three quantum coherence is without phase dispersion after the second gradient pulse of duration $3\tau_g$.

Pure-phase peak shapes are obtained with the experiment shown in Figure 2.7, as both coherence orders ($p = \pm 1$) during the evolution period are retained. For the distinction of positive and negative ω_2 frequencies quadrature phase detection is needed, while time proportional phase incrementation (TPPI)[21] allows the distinction between positive and negative ω_1 frequencies. This gradient-enhanced experiment leads to a reduction in the sensitivity by a factor 2 compared with an experiment with coherence order selection by phase cycling, because only half of the pathways allowed in Figure 2.6 are retained in Figure 2.7.

2.5 BUILDING BLOCKS FOR MULTIDIMENSIONAL NMR EXPERIMENTS

The building blocks consist of composites of free precession periods and periods with applied rf fields. In special cases, switched dc magnetic or electric fields, temperature and pressure jumps, optical irradiation, and variable angle sample spinning may also be involved. Often, the time dependence introduced by sample spinning has to be taken explicitly into account, and then synchronization of the rf pulses and of the sampling process with the sample rotation has to be considered.

It is usually possible to concentrate, at first, on the pulse sequence, irrespective of whether the selection of the coherence transfer pathways is achieved by phase cycling or by field gradient pulses. Sometimes, however, the coherence transfer pathway selection scheme is an integral part of the building blocks, and affects the pulse sequence design directly.

Both the E (evolution) and T (transfer) blocks can be characterized by an average Hamiltonian $\hat{\bar{\mathcal{H}}}_r$ and a corresponding relaxation or chemical exchange superoperator $\hat{\bar{\Gamma}}_r$ which together determine the development of the density operator of the spin system within the building blocks. The only important difference between the E and T blocks is that the time parameter t_r in an $E^{(r)}$ block is used as a time variable which is incremented from experiment to experiment within a multidimensional experiment sequence, while the time parameter τ_r in a $T^{(r)}$ block is kept constant over the entire experiment. There are also cases where even this distinction breaks down and where within a $T^{(r)}$ block a variable time parameter is used, for example for the suppression of undesired terms, such as zero quantum coherence in cross relaxation periods.[25,26] In the following, some simple building blocks are briefly discussed.

2.5.1 Rotations $\hat{T}^{(r)} = \exp\{-i\beta\hat{F}_q\}$

The index q indicates the rotation axis which may be $q = x, y, z$ or may represent an arbitrarily inclined axis. Rotations are the most frequently used transfer-block elements. The first transfer block $\hat{T}^{(1)}$ in a sequence, serving as a 'preparation period', often uses just a single $\pi/2$ pulse for the creation of coherence. In correlation experiments,[1,6,16] the 'mixing period' consists of a transfer block with one or several rf pulses. Usually, the pulses are considered to act instantaneously, so that relaxation can be neglected. Often the pulses are 'nonselective', in the sense that they affect all (homonuclear) spins equally.

In special cases, rf pulses with amplitude ω_1 and a variable rotation angle $\beta = \omega_1 t_r$ may also represent an $E^{(r)}$ block, for example in an experiment for measuring the spatial rf field distribution, such as in rotating frame imaging.[27]

2.5.2 Unperturbed Hamiltonian $\hat{\bar{\mathcal{H}}}_r = \mathcal{H}_0$

In many basic multidimensional experiments, all $E^{(r)}$ blocks use $\hat{\bar{\mathcal{H}}}_r = \mathcal{H}_0$. The frequency spread is then determined in all dimensions by the natural NMR spectrum, and the cross peaks map the transfer matrices of the T blocks in the eigenbasis of the Hamiltonian superoperator $\hat{\mathcal{H}}_0$, the eigenvalues

of which are the corresponding transition frequencies. Multidimensional spectra possess specific symmetry properties,[28,29] but these are lost when the average Hamiltonians of the different $E^{(r)}$ blocks are unequal.

2.5.3 Spin Coupling Hamiltonian $\hat{\bar{\mathcal{H}}}_r = \mathcal{H}_{\mathrm{II}}$

In some experiments, it is desirable to suppress the Zeeman interaction and to retain exclusively the scalar spin–spin coupling. In the case of weak coupling, this can be achieved by a π refocusing pulse applied in the center of the building block (Figure 2.8), which leads to

$$\hat{\bar{\mathcal{H}}}_r = \hat{\mathcal{H}}_{\mathrm{II}} = \sum_{k,l} 2\pi J_{kl} \hat{I}_{kz} \hat{I}_{lz} \qquad (2.28)$$

It should be noted that the effect of the π pulse on the density operator remains, and that the following equivalence holds:

$$\xrightarrow{\hat{\mathcal{H}}_0 t_r/2} \xrightarrow{(\pi)_x} \xrightarrow{\hat{\mathcal{H}}_0 t_r/2} \equiv \xrightarrow{\hat{\mathcal{H}}_{\mathrm{II}} t_r} \xrightarrow{(\pi)_x} \qquad (2.29)$$

Here and in the following we use the arrow notation introduced by Sørensen *et al*.[30] The term on top of the arrow indicates the phase operator in the exponent of a propagator, e.g. $\xrightarrow{\hat{\mathcal{H}}_0 t_r/2}$ is equivalent to the propagator $\exp\{-\mathrm{i}\hat{\mathcal{H}}_0 t_r/2\}$, and $\xrightarrow{(\pi)_x}$ is equivalent to $\exp\{-\mathrm{i}\pi\hat{F}_x\}$. Obviously, the effects of the $(\pi)_x$ pulse in equation (2.29) can be compensated for by appending another $(\pi)_x$ pulse at the end of the building block. Often this is irrelevant. The building block shown in Figure 2.8 is used as the evolution block in J-resolved spectroscopy.[31] It is also used in relayed coherence transfer,[32] and in multiple quantum spectroscopy.[33] In the latter two cases, the precession period is sandwiched between two $(\pi/2)_x$ pulses, which gives rise to the average Hamiltonian:

$$\hat{\bar{\mathcal{H}}}_r = \sum_{k<l} 2\pi J_{kl} \hat{I}_{ky} \hat{I}_{ly} \qquad (2.30)$$

Here, the three pulses compensate each other fully, adding up to 2π, and a pure bilinear rotation Hamiltonian remains.

2.5.4 Zeeman Hamiltonian $\hat{\bar{\mathcal{H}}}_r = \mathcal{H}_{\mathrm{I}}$

With the simplicity of tailoring a pure spin-coupling Hamiltonian $\hat{\bar{\mathcal{H}}}_r = \mathcal{H}_{\mathrm{II}}$ in mind, it appears to be equally easy to obtain a pure Zeeman Hamiltonian $\hat{\bar{\mathcal{H}}}_r = \mathcal{H}_{\mathrm{I}}$. However, in general, this is a difficult if not impossible task, as it requires the selective suppression of $\hat{\mathcal{H}}_{\mathrm{II}}$. The latter is, however, as a scalar interaction, invariant under any rotation in the three-dimensional space, and nonselective pulses or rf fields cannot be used to manipulate $\hat{\mathcal{H}}_{\mathrm{II}}$. This is equivalent to the statement that homonuclear broadband decoupling is not feasible by a direct tailoring of the average Hamiltonian $\hat{\bar{\mathcal{H}}}_r$. Other, less direct means have to be used to obtain $\hat{\bar{\mathcal{H}}}_r = \mathcal{H}_{\mathrm{I}}$.

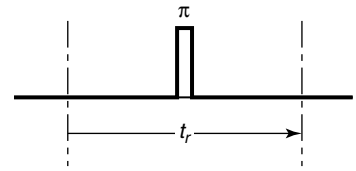

Figure 2.8. A building block with refocused chemical shift evolution obtained by the application of a nonselective π pulse in the center.

A first possibility is to use isotopic dilution, retaining in the average only one spin of a particular kind per molecule. This eliminates the homonuclear spin interactions, and the heteronuclear couplings can be rendered ineffective by standard CW or pulsed heteronuclear spin decoupling.[34,35] It is also possible to eliminate homonuclear couplings by a homonuclear decoupling scheme that uses selective irradiation of the coupling partners.

Another possible way to eliminate heteronuclear spin splittings is to apply an isotope-selective π pulse to the coupling partners at the center of an evolution interval $E^{(r)}$.[36,37] This interchanges coherence components within the multiplets and initiates refocusing of the heteronuclear multiplet evolution. Obviously this procedure cannot be applied during the detection period, because for each sampling point the π pulse would have to be positioned differently.

Sometimes, 'constant time evolution' is applied for homonuclear spin decoupling,[38] as illustrated in Figure 2.9. Keeping the evolution time T_r constant and varying in a systematic manner the position t_r' of a nonselective π pulse positioned within this interval, it is possible to define the variable $t_r = T_r - 2t_r'$ which governs exclusively the chemical shift evolution:

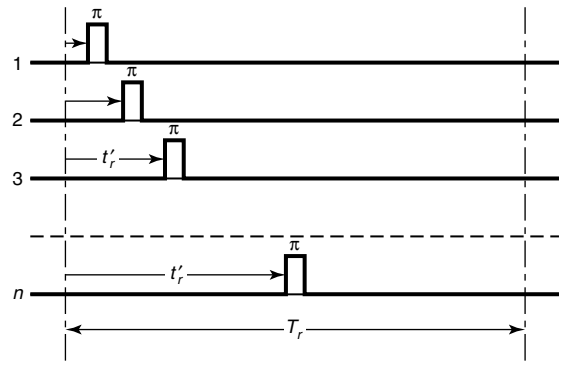

Figure 2.9. Constant time experiment for homonuclear spin decoupling. Instead of varying the length of an evolution period t_r, the total evolution time T_r is kept constant while a π pulse is shifted from $t_r' = 0$ to $t_r' = T_r/2$. The time variable t_r is then defined by $t_r = T_r - 2t_r'$.

$$\hat{\sigma}(t=0) \xrightarrow{\hat{\mathcal{H}}_{\mathrm{II}} T_r} \xrightarrow{\pi_x} \xrightarrow{\hat{\mathcal{H}}_{\mathrm{I}} t_r} \hat{\sigma}(t_r, T_r) \quad (2.31)$$

Obviously, the effect of $\hat{\mathcal{H}}_{\mathrm{II}}$ is not fully eliminated, although it no longer influences the time evolution in t_r. However, it contributes a T_r-dependent transformation that leads to J-coupling-dependent phase shifts. The occurrence of these phase shifts usually requires the plotting of magnitude spectra.

In solids where the scalar spin–spin interaction is negligible in comparison to the much stronger magnetic dipolar interaction, homonuclear decoupling is more straightforward. Due to the second rank tensor character of the dipolar interaction, it is possible to achieve homonuclear spin decoupling by means of multiple pulse sequences[39–41] and by high speed magic angle sample spinning.[42] Multiple pulse sequences normally simultaneously reduce the chemical shift spread by scaling,[39–41] while magic angle sample spinning also eliminates the chemical shielding anisotropy.[43,44]

There is a considerable number of further other building blocks in the arsenal of the advanced NMR spectroscopist. Among others, these include evolution blocks for scaling interactions,[45,46] transfer blocks for cross polarization,[47,48] blocks for various types of coherence transfer,[49–51] and transfer blocks for the creation of multiple quantum coherence.[16,32,33] It is not the purpose of this chapter to describe these blocks here. Rather, we discuss below a specific example of a reasonably complex three-dimensional experiment.

2.6 EXAMPLE OF A MULTIDIMENSIONAL NMR EXPERIMENT: ^{15}N–^{15}N CHEMICAL SHIFT CORRELATION FOR THE SEQUENTIAL ASSIGNMENT IN PROTEINS

(Co-authors: Serge Boentges and Jürgen M. Schmidt)

The features of multidimensional NMR are here exemplified by a novel experiment[52] designed for the assignment of backbone resonances in proteins.[53] A prerequisite is a ^{15}N-labeled protein sample. The three-dimensional experiments described here, called XTONOX and XNOTOX, generate a map correlating ^{15}N resonances in sequentially adjacent or spatially neighboring amino acid residues. The two-dimensional map is spread in a third dimension by the resonances of directly bonded NH protons which also serve for high sensitivity detection.

The coherence transfer from $^{15}N_i$ to $^{15}N_k$ is established via a proton–proton TOCSY–NOESY (in the XTONOX experiment) or a NOESY–TOCSY relay step (in the XNOTOX experiment) bracketed by two INEPT transfers.[49] The two-step transfers are effective for typical β-sheet secondary structural elements, while in α-helices a direct proton–proton NOE transfer is more efficient. This leads to the following sequences of transfers for XTONOX:

$$^{15}N_i \xrightarrow{\text{INEPT}} NH_i \xrightarrow{\text{TOCSY}} C_\alpha H_i \xrightarrow{\text{NOESY}} NH_{i+1} \xrightarrow{\text{INEPT}} {}^{15}N_{i+1} \text{ for } \beta\text{-sheets}$$

and

$$^{15}N_i \xrightarrow{\text{INEPT}} NH_i \xrightarrow{\text{NOESY}} NH_{i\pm1} \xrightarrow{\text{INEPT}} {}^{15}N_{i\pm1} \text{ for } \alpha\text{-helices}$$

For XNOTOX the transfer pathways are:

$$^{15}N_i \xrightarrow{\text{INEPT}} NH_i \xrightarrow{\text{NOESY}} C_\alpha H_{i-1} \xrightarrow{\text{TOCSY}} NH_{i-1} \xrightarrow{\text{INEPT}} {}^{15}N_{i-1} \text{ for } \beta\text{-sheets}$$

and

$$^{15}N_i \xrightarrow{\text{INEPT}} NH_i \xrightarrow{\text{NOESY}} NH_{i\pm1} \xrightarrow{\text{INEPT}} {}^{15}N_{i\pm1} \text{ for } \alpha\text{-helices}$$

Both experiments start and end with an additional INEPT transfer to allow the usage and detection of proton magnetization for sensitivity enhancement. The two resulting pulse sequences are shown in Figure 2.10.

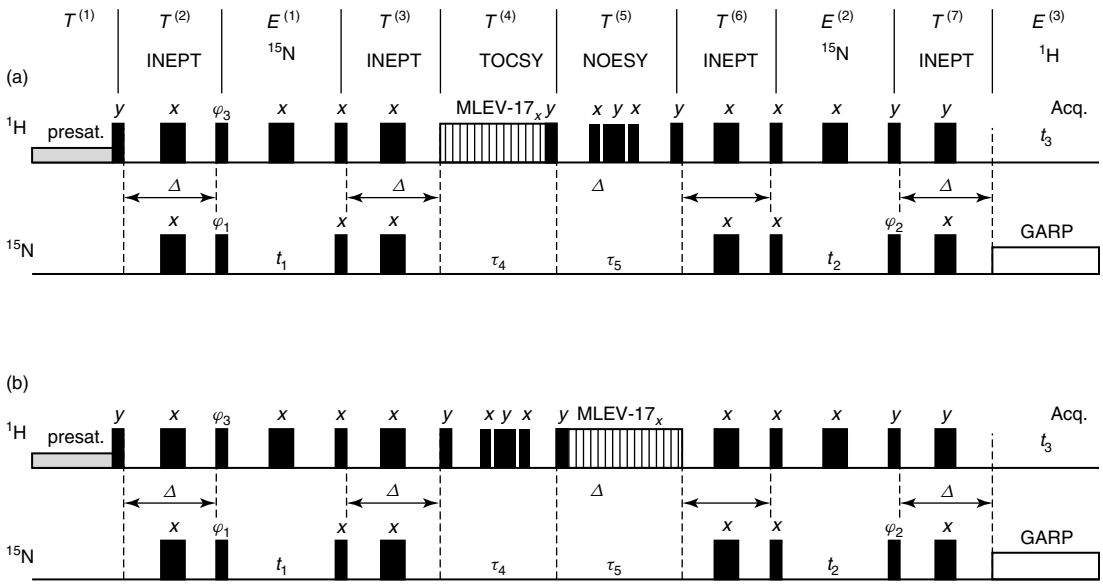

Figure 2.10. Pulse sequences for the XTONOX (a) and XNOTOX (b) experiments. The eight-step phase cycle used x phases with the signs (φ_1, φ_2, φ_3, acquisition): $(++++)$, $(-++-)$, $(+-+-)$, $(--+-)$, $(++-+)$, $(-+-+)$, $(+--+)$, and $(----)$.[52] In addition, TPPI is applied to φ_1 and φ_2 to allow the distinction of positive and negative frequencies in ω_1 and ω_2.

We will now analyze the XTONOX sequence in more detail. As can be seen from Figure 2.10, the sequence consists of seven transfer periods $T^{(1)}, \ldots, T^{(7)}$ and three evolution periods $E^{(1)}$, $E^{(2)}$, and $E^{(3)}$. The initial transfer period $T^{(1)}$ incorporates a selective saturation sequence applied to the water resonance for reducing the intensity of the disturbing water signal. For the other protons, transverse magnetization is created by a $(\pi/2)_y^I$ pulse. We concentrate here on the ^{15}NH subsystem and use I for the proton spin and S for the ^{15}N spin. Then

$$\hat{I}_z \xrightarrow{T^{(1)}} \hat{I}_x \tag{2.32}$$

The transfer period $T^{(2)}$ consists of a standard INEPT[49] transfer from ^{1}H to ^{15}N, for enhancing the magnetization of the latter spin. The sequence of operations can be written in the form

$$\hat{\sigma}' \xrightarrow{2\pi J_{IS}\hat{I}_z\hat{S}_z\Delta} \xrightarrow{(\pi/2)_x^{I+S}} \hat{\sigma}'' \tag{2.33}$$

The pair of π pulses in the center of $T^{(2)}$ refocuses the chemical shift effects, as described before. The remaining phase inversion effect, which is apparent in equation (2.29), has been integrated into the phase of the $(\pi/2)_x^{I+S}$ pulse pair in equation (2.33). The transformation of equation (2.33) can be rewritten as

$$\hat{\sigma}'(\xrightarrow{(\pi/2)_x^{I+S}}) \xrightarrow{2\pi J_{IS}\hat{I}_y\hat{S}_y\Delta} \hat{\sigma}'' \tag{2.34}$$

Applying this to the result of the transfer $T^{(1)}$ [equation (2.32)], it is obvious that the $(\pi/2)_x^{I+S}$ pulse pair in equation (2.34) has no effect, and can be disregarded. The effect of $T^{(2)}$ is thus a bilinear rotation:

$$\begin{aligned}\hat{I}_x &\xrightarrow{T^{(2)}} \hat{I}_x \cos(\pi J_{IS}\Delta) \\ &-2\hat{I}_z\hat{S}_y \sin(\pi J_{IS}\Delta)\end{aligned} \tag{2.35}$$

and the maximum antiphase S spin coherence $2\hat{I}_z\hat{S}_y$ is obtained for $\Delta = 1/(2J_{IS})$.

The I-spin π pulse applied in the middle of the first evolution period $E^{(1)}$ refocuses I-spin chemical shift effects, as described above, but, more importantly, also refocuses the heteronuclear J-coupling effects. For the ^{15}N evolution, a pure chemical shift average Hamiltonian remains,

$$\hat{\bar{\mathcal{H}}}^{(1)} = \Omega_S\hat{S}_z \tag{2.36}$$

and the ^{15}N antiphase coherence evolves as

$$2\hat{I}_z\hat{S}_y \xrightarrow{\hat{\hat{\mathcal{H}}}^{(1)}t_1} 2\hat{I}_z(\hat{S}_y\cos\Omega_S t_1 - \hat{S}_x\sin\Omega_S t_1) \qquad (2.37)$$

This is responsible for the frequency spread along the ω_1 axis in the three-dimensional XTONOX spectrum, and characterizes the origin spin $^{15}N_i$.

The coherence transfer to spin $^{15}N_{i\pm1}$ (see above) proceeds by the four transfer steps $T^{(3)}$, $T^{(4)}$, $T^{(5)}$, and $T^{(6)}$. The two INEPT steps $T^{(3)}$ and $T^{(6)}$ are fully analogous to the transfer $T^{(2)}$. The crucial processes are $T^{(4)}$ and $T^{(5)}$. The application of a CW or pulsed (e.g MLEV-17) rf field during the TOCSY period $T^{(4)}$ of duration τ_4 causes a suppression of the proton chemical shift and heteronuclear J-coupling effects.[54,55] The Hamiltonian relevant for the evolution of the proton magnetization is then (expressed in a frame rotating with the rf frequency ω_{rf})

$$\hat{\hat{\mathcal{H}}}^{(4)} = \sum_{kl} 2\pi J_{kl}\hat{\boldsymbol{I}}_k\cdot\hat{\boldsymbol{I}}_l + \omega_1\sum\hat{I}_{kx} \qquad (2.38)$$

The first term causes isotropic mixing and a transfer of spin order between the different proton spins within one amino acid residue, while the second term with the rf amplitude ω_1 functions as a phase selection operator which selects the x phase. The most relevant transfer effected by the Hamiltonian of equation (2.38) is[54]

$$\begin{aligned}\hat{I}_{NH,x} \xrightarrow{T^{(4)}} &\tfrac{1}{2}\hat{I}_{NH,x}[1+\cos(2\pi J_{NH,C_\alpha H}\tau_4)]\\ &+\tfrac{1}{2}\hat{I}_{C_\alpha H,x}[1-\cos(2\pi J_{NH,C_\alpha H}\tau_4)]\\ &+(\hat{I}_{NH,y}\hat{I}_{C_\alpha H,z}-\hat{I}_{NH,z}\hat{I}_{C_\alpha H,y})\\ &\sin(2\pi J_{NH,C_\alpha H}\tau_4)\end{aligned} \qquad (2.39)$$

This leads to a transfer of the NH proton magnetization to $C_\alpha H$ proton magnetization. At the same time, transfers of magnetization to the side-chain protons are also taking place.

The transfer block $T^{(5)}$ consists of a cross-relaxation period, bracketed by two $(\pi/2)_y$ pulses that convert transverse x magnetization into longitudinal z magnetization, and vice versa. During the time τ_5, the relaxation superoperator $\hat{\hat{\Gamma}}$ is acting and $T^{(5)}$ causes, among other things, a transfer

$$\begin{aligned}\hat{I}_{C_\alpha H_i,x} \xrightarrow{T^{(5)}} &\hat{I}_{C_\alpha H_i,x}\tfrac{1}{2}[1+\exp(-\Gamma_{i+1,i}\tau_5)]\\ &+\hat{I}_{NH_{i+1},x}\times\tfrac{1}{2}[1-\exp(-\Gamma_{i+1,i}\tau_5)]\end{aligned} \qquad (2.40)$$

to a sequentially (or spatially) neighboring amino acid residue. The central composite π pulse is beneficial for the minimization of the water signal: by inversion, a recovery of the water magnetization during τ_5 is prevented.[56] The following steps ($E^{(2)}$, $T^{(7)}$, and $E^{(3)}$) proceed analogously, and do not require further comment.

A decisive advantage of the XTONOX and XNOTOX experiments for backbone assignment is the correlation of single ^{15}N resonances for each amino acid residue (except for some additional side-chain N^{15} resonances). This leads to simple, often well resolved spectra that are amenable to automated computer analysis. The additional three-dimensional spread by the NH resonances provides further enhanced resolution. The resulting three-dimensional spectrum has a characteristic appearance that is sketched in Figure 2.11. If we consider a particular pair $^{15}N_i$ and $^{15}N_k$, each of the planes defined by $\omega_3 = \Omega_{NH_i}$ and $\omega_3 = \Omega_{NH_k}$ contains a diagonal peak at $\omega_1 = \omega_2 = \Omega_{N_i}$ or Ω_{N_k}, respectively. For the β-sheet neighborhood and the XTONOX experiment, only the plane $\omega_3 = \Omega_{NH_k}$ contains a cross peak at $\omega_1 = \Omega_{N_i}$, $\omega_2 = \Omega_{N_k}$ when $k = i+1$. No corresponding cross peak is found in the plane $\omega_3 = \Omega_{NH_i}$. However, the cross peak $\omega_1 = \Omega_{N_k}$, $\omega_2 = \Omega_{N_i}$ is found in the plane $\omega_1 = \Omega_{N_k}$, $\omega_2 = \Omega_{N_i}$ in the XNOTOX spectrum. For an α-helix neighborhood, each of the $\omega_3 = \Omega_{NH_k}$ planes for $k = i \pm 1$ contains a cross peak. This allows the distinction of secondary structural elements.

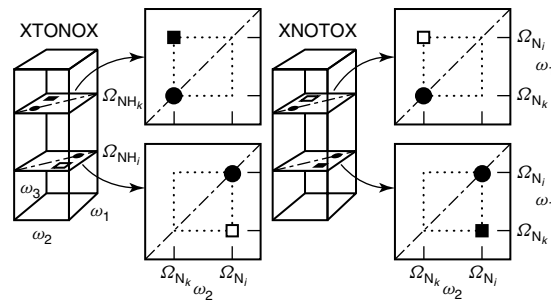

Figure 2.11. Schematic representation of the diagonal and cross-peak pattern in XTONOX and XNOTOX three-dimensional spectra. The 3D spectra and two representative ω_3 sections with constant Ω_{NH} frequency are shown. For β-sheet structural elements, $k = i + 1$ holds and only the black diagonal and cross peaks appear because the TOCSY–NOESY and NOESY–TOCSY transfers are unidirectional. For α-helical structural elements, $k = i \pm 1$ and all the indicated peaks can appear because here there is a one-step NOESY transfer which has no directionality. The same is true for long-range cross peaks.

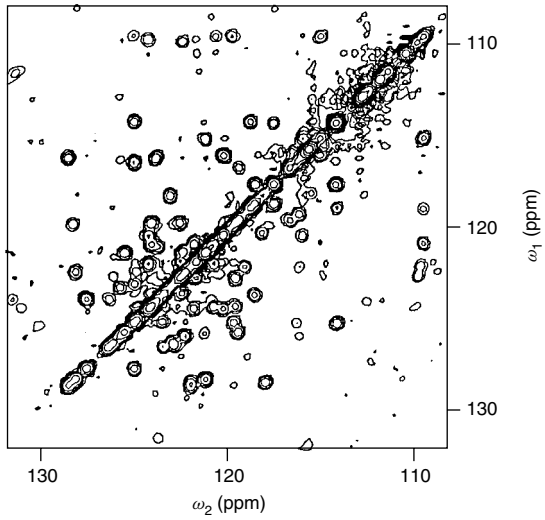

Figure 2.12. Skyline projection along ω_3 of a 500 MHz XNOTOX three-dimensional spectrum of a 2.65 mM solution of 99% ^{15}N-labeled human ubiquitin in 95% H_2O, 5% D_2O.[51] The spectrum shows the $^{15}N-^{15}N$ connectivities essential for the sequential assignment given in Figure 2.13.

The XTONOX/XNOTOX experiment has been applied to ^{15}N-labeled human ubiquitin (Figure 2.12). A sizable fraction of the amino acid sequence could be determined without problems by using a computer analysis procedure.[52] Two equivalent stretches of assignment steps based on two-dimensional sections from XTONOX and XNOTOX spectra are shown in Figure 2.13.

Naturally, the sequential assignment is interrupted by proline residues which lack the NH proton required for observation, and ambiguities occur when unidentified long-range correlations between sequentially remote but spatially neighboring residues appear. In these cases, it is necessary to make recourse to a standard primary sequence determination and to an identification of the $^{15}N_k$ and NH_k resonances by the characteristic side-chain resonances. Due to the TOCSY step in the two experiments, the required cross peaks to the side chains are also contained in the XTONOX and XNOTOX spectra.

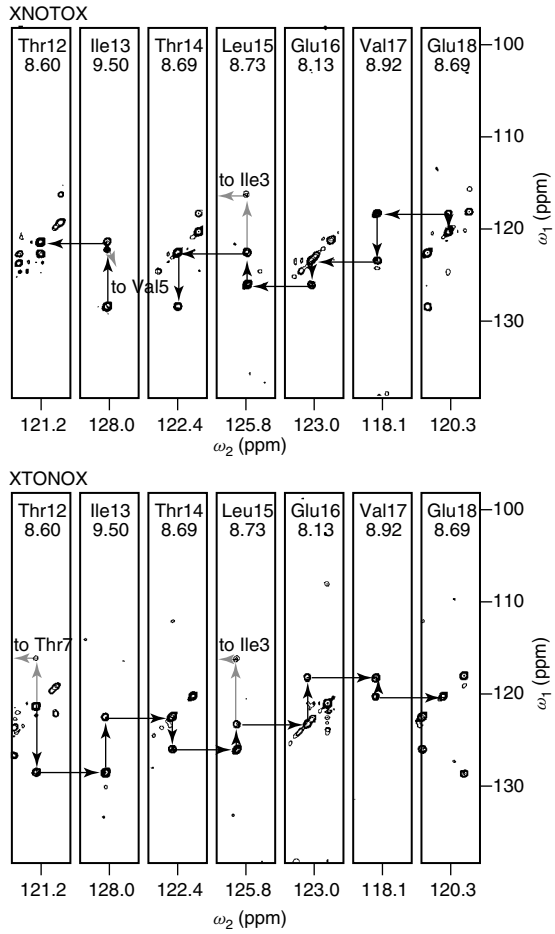

Figure 2.13. Sequential assignment in ^{15}N-labeled human ubiquitin based on (ω_1, ω_2) sections from 500 MHz three-dimensional XTONOX and XNOTOX ^{15}N spectra. Assignments are indicated for the second strand of the β-sheet region between Thr12 and Glu18. Additional long-range cross peaks appear for Leu15–Ile3, Ile–Val5, and Thr12–Thr7 which are due to NOE transfer only, and confirm the spatial vicinity of a further β-strand with the residues 1–7.[57]

2.7 OUTLOOK

Multidimensional spectroscopy is more than just a powerful assignment technique. It opens up a new world of experimental design. It is not so much the display of multidimensional maps but rather the type of underlying time domain experiments which is novel. The possibility of introducing several time variables in a complex experimental procedure provides a multitude of approaches that can be adapted to almost any conceivable practical situation.

RELATED ARTICLES IN THE ENCYCLOPEDIA OF MAGNETIC RESONANCE

Double Quantum Coherence

Early NMR Experiences and Experiments

Fourier Transform Spectroscopy

Liouville Equation of Motion

Multiple Quantum Coherence Imaging

Nuclear Overhauser Effect

Polarization Transfer Experiments via Scalar Coupling in Liquids

Selective NOESY

Stochastic Excitation

Two-Dimensional Powder Correlation Methods

REFERENCES

1. R. R. Ernst, G. Bodenhausen, and A. Wokaun, *Principles of Nuclear Magnetic Resonance in One and Two Dimensions*, Clarendon, Oxford, 1987.
2. A. Bax, *Two-Dimensional NMR in Liquids*, Delft University/Reidel, Dortrecht, 1982.
3. Atta-ur Rahman, *Nuclear Magnetic Resonance, Basic Principles*, Springer, New York, 1986; N. Chandrakumar and S. Subramanian, *Modern Techniques in High Resolution FT-NMR*, Springer, New York, 1987; H. Friebolin, *Ein-und zweidimensionale NMR-Spektroskopie*, VCH, Weinheim, 1988; *Basic One- and Two-Dimensional NMR*, VCH, Weinheim, 1991; G. E. Martin and A. S. Zekter, *Two-Dimensional NMR Methods for Establishing Molecular Connectivity*, VCH, Weinheim, 1988; J. Schraml and J. M. Bellama, *Two-Dimensional NMR Spectroscopy*, Wiley Interscience, New York, 1988; W. S. Brey (ed.), *Pulse Methods in 1D and 2D Liquid-Phase NMR*, Academic, New York, 1988.
4. M. Goldman, *Quantum Description of High-Resolution NMR in Liquids*, Clarendon, Oxford, 1988; G. D. Mateescu and A. Valeriu, *2D NMR, Density Matrix and Product Operator Treatment*, PTR/Prentice Hall, Englewood Cliffs, NJ, 1993.
5. E. L. Hahn, *Phys. Rev.*, 1950, **80**, 580.
6. J. Jeener, *Ampère Summer School*, Basko Polje, Yugoslavia, 1971, unpublished.
7. T. Sleator, E. L. Hahn, C. Hilbert, and J. Clarke, *Phys. Rev. Lett.*, 1985, **55**, 1742; *Phys. Rev., B*, 1987, **36**, 1969.
8. M. A. McCoy and R. R. Ernst, *Chem. Phys. Lett.*, 1989, **159**, 587.
9. W. A. Anderson and R. Freeman, *J. Chem. Phys.*, 1962, **37**, 85.
10. R. Freeman and W. A. Anderson, *J. Chem. Phys.*, 1962, **37**, 2053.
11. R. A. Hoffman and S. Forsén, *Prog. NMR Spectrosc.*, 1966, **1**, 15.
12. R. R. Ernst and W. A. Anderson, *Rev. Sci. Instrum.*, 1966, **37**, 93.
13. R. R. Ernst, *Adv. Magn. Reson.*, 1966, **2**, 1.
14. T. C. Farrar and E. D. Becker, *Pulse and Fourier Transform NMR*, Academic, New York, 1971.
15. D. Shaw, *Fourier Transform NMR Spectroscopy*, 2nd edn, Elsevier, Amsterdam, 1984.
16. W. P. Aue, E. Bartholdi, and R. R. Ernst, *J. Chem. Phys.*, 1976, **64**, 2229.
17. G. Bodenhausen and R. R. Ernst, *J. Magn. Reson.*, 1981, **45**, 367.
18. A. D. Bain, *J. Magn. Reson.*, 1984, **56**, 418.
19. G. Bodenhausen, H. Kogler, and R. R. Ernst, *J. Magn. Reson.*, 1984, **58**, 370.
20. A. Wokaun and R. R. Ernst, *Chem. Phys. Lett.*, 1977, **52**, 407.
21. G. Drobny, A. Pines, S. Sinton, D. Weitekamp, and D. Wemmer, *Faraday Div. Chem. Soc. Symp.*, 1979, **13**, 49; G. Bodenhausen, R. L. Vold, and R. R. Vold, *J. Magn. Reson.*, 1980, **37**, 93.
22. A. A. Maudsley, A. Wokaun, and R. R. Ernst, *Chem. Phys. Lett.*, 1978, **55**, 9.
23. R. E. Hurd, *J. Magn. Reson.*, 1990, **87**, 422.
24. J. Ruiz-Cabello, G. W. Vuister, C. T. W. Moonen, P. Van Gelderen, J. S. Cohen, and P. C. M. Van Zijl, *J. Magn. Reson.*, 1992, **100**, 282.
25. S. Macura, Y. Huang, D. Suter, and R. R. Ernst, *J. Magn. Reson.*, 1981, **43**, 259.
26. S. Macura, K. Wüthrich, and R. R. Ernst, *J. Magn. Reson.*, 1982, **46**, 269.
27. D. I. Hoult, *J. Magn. Reson.*, 1979, **33**, 183.

28. C. Griesinger, C. Gemperle, O. W. Sørensen, and R. R. Ernst, *Mol. Phys.*, 1987, **62**, 295.
29. S. Boentges, B. U. Meier, C. Griesinger, and R. R. Ernst, *J. Magn. Reson.*, 1989, **85**, 337.
30. O. W. Sørensen, G. W. Eich, M. H. Levitt, G. Bodenhausen, and R. R. Ernst, *Progr. NMR Spectrosc.*, 1983, **16**, 163.
31. W. P. Aue, J. Karhan, and R. R. Ernst, *J. Chem. Phys.*, 1976, **64**, 4226.
32. G. Eich, G. Bodenhausen, and R. R. Ernst, *J. Am. Chem. Soc.*, 1982, **104**, 3731.
33. S. Vega, T. W. Shattuck, and A. Pines, *Phys. Rev. Lett.*, 1976, **37**, 43; L. Braunschweiler, G. Bodenhausen, and R. R. Ernst, *Mol. Phys.*, 1983, **48**, 535.
34. R. R. Ernst, *J. Chem. Phys.*, 1966, **45**, 3845.
35. M. H. Levitt, R. Freeman, and T. Frenkiel, *Adv. Magn. Reson.*, 1983, **11**, 47.
36. A. Kumar and R. R. Ernst, *J. Magn. Reson.*, 1976, **24**, 425.
37. L. Müller, A. Kumar, and R. R. Ernst, *J. Magn. Reson.*, 1977, **25**, 383.
38. A. Bax and R. Freeman, *J. Magn. Reson.*, 1981, **44**, 542.
39. J. S. Waugh, L. M. Huber, and U. Haeberlen, *Phys. Rev. Lett.*, 1968, **20**, 180.
40. U. Haeberlen, *High-Resolution NMR in Solids* (Adv. Magn. Reson., Suppl. 1), Academic Press, New York, 1976.
41. M. Mehring, *High Resolution NMR Spectroscopy in Solids*, 2nd edn., Springer, Berlin, 1983.
42. E. R. Andrew, *Progr. NMR Spectrosc.*, 1971, **8**, 1.
43. C. A. Fyfe, *Solid State NMR for Chemists*, CFC, Guelph, Ontario, 1983.
44. B. C. Gerstein and C. R. Dybowski, *Transient Techniques in NMR of Solids*, Academic, New York, 1985.
45. J. D. Ellett and J. S. Waugh, *J. Chem. Phys.*, 1969, **51**, 2851.
46. W. P. Aue and R. R. Ernst, *J. Magn. Reson.*, 1978, **31**, 533.
47. S. R. Hartmann and E. L. Hahn, *Phys. Rev.*, 1962, **128**, 2042.
48. A. Pines, M. G. Gibby, and J. S. Waugh, *J. Chem. Phys.*, 1973, **59**, 569.
49. G. A. Morris and R. Freeman, *J. Am. Chem. Soc.*, 1979, **101**, 760.
50. D. P. Burum and R. R. Ernst, *J. Magn. Reson.*, 1980, **39**, 163.
51. D. M. Doddrell, D. T. Pegg, and M. R. Bendall, *J. Magn. Reson.*, 1982, **48**, 323.
52. S. Boentges, Dissertation, ETH, Zürich, Switzerland, 1994.
53. K. Wüthrich, *NMR of Proteins and Nucleic Acids*, Wiley, New York, 1986.
54. L. Braunschweiler and R. R. Ernst, *J. Magn. Reson.*, 1983, **53**, 521.
55. D. G. Davis and A. Bax, *J. Am. Chem. Soc.*, 1985, **107**, 2820.
56. L. Müller, S. Campbell-Burk, and P. Domaille, *J. Magn. Reson.*, 1992, **96**, 408.
57. S. Vijay-Kumar, C. Brugg, and W. J. Cook, *J. Mol. Biol.*, 1987, **194**, 531.